

Comparison of sequencing-based methods to profile DNA methylation and identification of monoallelic epigenetic modifications

R Alan Harris^{1,*}, Ting Wang², Cristian Coarfa¹, Raman P Nagarajan³, Chibo Hong³, Sara L Downey³, Brett E Johnson³, Shaun D Fouse³, Allen Delaney⁴, Yongjun Zhao⁴, Adam Olshen³, Tracy Ballinger⁵, Xin Zhou², Kevin J Forsberg², Junchen Gu², Lorigail Echipare⁶, Henriette O'Geen⁶, Ryan Lister⁷, Mattia Pelizzola⁷, Yuanxin Xi⁸, Charles B Epstein⁹, Bradley E Bernstein^{9,11}, R David Hawkins¹², Bing Ren^{12,13}, Wen-Yu Chung^{14,15}, Hongcang Gu⁹, Christoph Bock^{9,16–18}, Andreas Gnirke⁹, Michael Q Zhang^{14,15}, David Haussler⁵, Joseph R Ecker⁷, Wei Li⁸, Peggy J Farnham⁶, Robert A Waterland^{1,19}, Alexander Meissner^{9,16,17}, Marco A Marra⁴, Martin Hirst⁴, Aleksandar Milosavljevic¹ & Joseph F Costello³

Analysis of DNA methylation patterns relies increasingly on sequencing-based profiling methods. The four most frequently used sequencing-based technologies are the bisulfite-based methods MethylC-seq and reduced representation bisulfite sequencing (RRBS), and the enrichment-based techniques methylated DNA immunoprecipitation sequencing (MeDIP-seq) and methylated DNA binding domain sequencing (MBD-seq). We applied all four methods to biological replicates of human embryonic stem cells to assess their genome-wide CpG coverage, resolution, cost, concordance and the influence of CpG density and genomic context. The methylation levels assessed by the two bisulfite methods were concordant (their difference did not exceed a given threshold) for 82% for CpGs and 99% of the non-CpG cytosines. Using binary methylation calls, the two enrichment methods were 99% concordant and regions assessed by all four methods were 97% concordant. We combined MeDIP-seq with methylation-sensitive restriction enzyme (MRE-seq) sequencing for comprehensive methylome coverage at lower cost. This, along with RNA-seq and ChIP-seq of the ES cells enabled us to detect regions with allele-specific epigenetic states, identifying most known imprinted regions and new loci with monoallelic epigenetic marks and monoallelic expression.

DNA methylation plays a vital role in embryonic development, maintenance of pluripotency, X-chromosome inactivation and genomic imprinting through regulation of transcription, chromatin structure and chromosome stability¹. It occurs at the C5 position of cytosines within CpG dinucleotides^{2–4} and at non-CpG cytosines in plants and embryonic stem cells (ESCs) in mammals. 5-Hydroxymethylation of cytosine also occurs in certain human and mouse cells^{5,6} and is catalyzed by Tet proteins acting on methylated cytosine⁷. Several

experimental methods detect methylation but not hydroxymethylation, whereas others detect both but cannot distinguish them.

Understanding the role of DNA methylation in development and disease requires knowledge of the distribution of these modifications in the genome. The availability of reference genome assemblies and massively parallel sequencing has led to methods that provide high-resolution, genome-wide profiles of 5-methylcytosine^{8–16}. In contrast to arrays, sequencing-based methods can interrogate DNA methylation in repetitive sequences and more readily allow epigenetic states to be assigned to specific alleles. The unique characteristics of each method leave uncertainty about how to select the method best suited to answer particular biological questions. DNA methylation maps are being produced by many laboratories worldwide, and their integration forms a basis for emerging international epigenome projects¹⁷. Thus, it is critical to determine the precision of each method, and how reliably they can be compared.

Here, we provide a detailed and quantitative comparison of four sequencing-based methods for genome-wide DNA methylation profiling. We focused on two methods that use bisulfite conversion (MethylC-seq⁸ and RRBS⁹), and two methods that use enrichment of methylated DNA (MeDIP-seq^{10,11} and MBD-seq¹²). We also developed an integrative methodology combining MeDIP-seq to detect methylated CpGs with MRE-seq^{13,14} to detect unmethylated CpGs. Unlike the enrichment methods alone, the integrative method can accurately identify regions of intermediate methylation which—in conjunction with single nucleotide polymorphism (SNP) profiling from the sequencing data—permits genome-wide identification of allele-specific epigenetic states.

RESULTS

Generation of DNA methylation profiles from human ESCs

Four individual sequencing-based methods and one integrative method were used to generate and compare DNA methylation profiles of three biological replicates of H1 ESCs. MethylC-seq (data used here is from ref. 8) involves shotgun sequencing of DNA treated with

*A full list of author affiliations appears at the end of the paper.

Published online 19 September 2010; doi:10.1038/nbt.1682

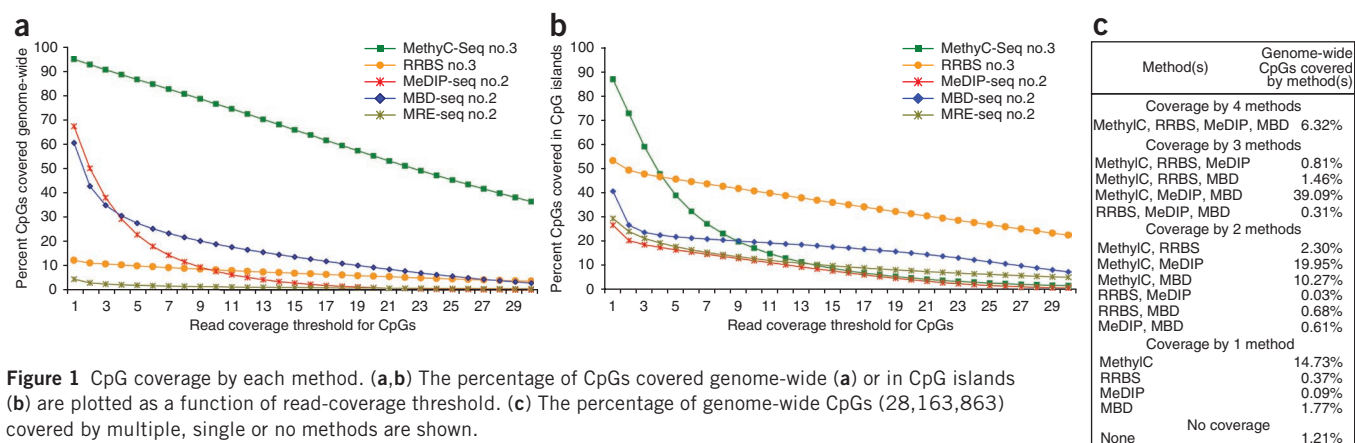


Figure 1 CpG coverage by each method. (a,b) The percentage of CpGs covered genome-wide (a) or in CpG islands (b) are plotted as a function of read-coverage threshold. (c) The percentage of genome-wide CpGs (28,163,863) covered by multiple, single or no methods are shown.

bisulfite, a chemical that converts unmethylated cytosines but not methylated cytosines to uracil. The second bisulfite-based method, RRBS⁹, reduces the portion of the genome analyzed through *MspI* digestion and fragment size selection. MeDIP-seq^{10,11} and MBD-seq¹² involve enrichment of methylated regions followed by sequencing. In MeDIP-seq, an anti-methylcytosine antibody is used to immunoprecipitate methylated single-stranded DNA fragments. MBD-seq uses the MBD2 protein methyl-CpG binding domain to enrich for methylated double-stranded DNA fragments. As a complementary approach for use in conjunction with methylated fragment enrichment methods, unmethylated CpGs are identified by sequencing size-selected fragments from parallel DNA digestions with the methyl-sensitive restriction enzymes (MREs) *HpaII* (C^ACGG), *Hin6I* (G^ACGC) and *Acil* (C^ACGC)(MRE-seq)¹³.

To reliably identify biological variation in methylation among samples from different individuals or biological states, one must determine the variation attributable to biological and technical replication. As an initial assessment of DNA methylation concordance among three H1 ESC biological replicates, the methylation status of 27,578 CpGs was assayed on the widely used bisulfite-based Infinium bead-array. The Infinium method involves bisulfite conversion and hybridization, rather than sequencing. The beta values, roughly representing CpG methylation levels, in the replicates were compared by calculating concordance correlation coefficients. The coefficients were very high, ranging from 0.992 to 0.996 (Supplementary Fig. 1). Replicate no. 1 and replicate no. 2 were run a second time on the Infinium platform to assess technical variation (data not shown). Most (98.9%) of the total variation (technical and biological) was technical. Thus, platform comparisons using these replicates should be very informative.

As a second and more comprehensive analysis of variation in methylation calls, RRBS, covering ~1.6 million CpGs, MeDIP-seq and MRE-seq was performed on all three biological replicates. The correlation between the biological replicates was high for RRBS (Supplementary Fig. 2) as it was for MeDIP-seq and MRE-seq (Supplementary Fig. 3). These results show that cell passage-related 'biological variation' in methylation is present but minimal on the scale of the genome. The rare biological variation in methylation levels was confirmed by pyrosequencing of selected loci (Supplementary Fig. 4 and Supplementary Table 1).

Several algorithms are available for bisulfite-treated short-read mapping, differences in which might alter local read density in a map, and ultimately affect methylation calls. Our assessment of overall concordance between aligners, including Bowtie¹⁸, BSMAP¹⁹,

Pash²⁰, RMAP²¹ and ZOOM²² applied to a subset of the MethylC-seq data⁹, indicated that, despite differences in speed and accuracy, aligner choice was unlikely to have a significant impact on the platform comparisons (Supplementary Table 2).

There are several important parameters in choosing an appropriate method for particular experimental goals, including the total number and local context of CpGs interrogated and the amount of sequencing required. To determine the impact of sequencing depth on coverage, we plotted CpG coverage genome-wide (Fig. 1a) and in CpG islands (Fig. 1b) as a function of read coverage threshold for CpGs. For MeDIP-seq and MBD-seq, the CpG coverage does not include CpGs for which a lack of methylation could be inferred from lack of reads (Fig. 1a,b). Thus, because CpG islands are predominantly unmethylated, the CpG coverage in CpG islands is lower for the enrichment methods than for either RRBS or MethylC-seq. As an indicator of the cost efficiency for each method, we also plotted the CpG coverage normalized to a single giga base pair (Gbp) of sequence depth in the methylome maps (Supplementary Fig. 5). Enrichment methods had the lowest cost per CpG covered genome-wide, whereas RRBS had the lowest cost per CpG covered in CpG islands. For the enrichment methods we examined the potential effect of CpG density on read coverage. Most of the genome is methylated and CpG poor, but a small fraction is unmethylated and CpG rich (that is, CpG island). Consistent with this, MeDIP-seq and MBD-seq enrich primarily for low CpG density regions, along with a small subset of methylated CpG islands. In contrast, MRE-seq interrogates higher CpG density regions because they have an abundance of unmethylated recognition sites for these enzymes. Therefore, the coverage of MRE-seq and enrichment methods is notably complementary (Supplementary Fig. 6).

A major advantage of the sequencing-based methods over microarrays is their ability to interrogate CpGs in repetitive elements. Approximately 45% of the human genome is derived from transposable elements, a major driving force in the evolution of mammalian gene regulation^{23,24}, with nearly half of all CpGs falling within these repetitive regions. The extent to which different sequencing-based methods interrogate repeats is therefore of considerable interest. In general, genome-wide CpG coverage (Fig. 1a) was proportional to CpG coverage in repeats (Table 1). The percent of interrogated CpGs in repeats was similar across all four methods, with MBD-seq capturing the highest fraction of repeat sequences (59.1%). Each of these methods is therefore useful for investigating this important and largely unexplored area. MRE-seq, however, only minimally interrogates repeats, consistent with their dense methylation.

Table 1 Critical parameters in sequencing-based DNA methylation profiling

Method	H1 DNA sample no.	Total bases generated (Gbp)	Total high quality bases (Gbp)	Total bases in map (Gbp)	Maximum resolution (bp)	1-read coverage of CpGs in repeats (no.,%)	Percentage of assayed CpGs in repeats (%)
MethylC-seq	no. 3	172.49	115	87.5	1	13,303,415 (91.8)	49.7
RRBS	no. 3	1.58	1.43	1.28	1	1,646,649 (11.4)	47.5
MeDIP-seq	no. 1	3.42	2.07	1.95	150	10,004,670 (68.3)	52.9
MeDIP-seq	no. 2	3.02	1.84	1.73	150	10,101,868 (68.9)	53.2
MeDIP-seq	nos. 1 + 2	6.44	3.91	3.68	150	11,693,059 (79.8)	53.5
MBD-seq	no. 2	5.67	3.71	2.21	150	10,080,007 (68.8)	59.1
MRE-seq	no. 1	3.61	1.31	0.96	1	306,635 (2.07)	21.7
MRE-seq	no. 2	4.03	1.69	1.3	1	232,885 (1.59)	18.6

Sequencing statistics and CpG coverage are shown for MethylC-seq (207 lanes, data analyzed here were from ref. 8.), RRBS (2 lanes), MeDIP-seq (4 lanes each), MBD-seq (3 lanes) and MRE-seq (3 lanes each). As the amount of sequence produced per lane is increasing, we also provide “Gbp of sequence” as a measure of the relative cost of each method. The methods differ significantly in total bases generated by the Illumina sequencer, total high-quality bases passing Illumina chastity filtering and mapping uniquely and total bases used for generating methylome maps (high-quality bases passing redundancy filters). The H1 replicates assayed and the Gbp of sequence at successive processing stages by each method are shown. The bisulfite-based methods and MRE-seq resolve the methylation status of individual cytosines, whereas the MeDIP-seq and MBD-seq read mappings are extended to 150 bp, resulting in a maximum resolution of 150 bp. This extension is applied to calculations of CpG coverage but is not applied to the Gbp of sequence at the processing stages. Coverage information is shown for repeats (primarily transposon sequences) genome-wide. Although maximum resolution of each method is reported, resolution can be assessed at various levels. As the level of resolution decreases, as a consequence of averaging of methylation scores over a window of larger size, for example, imperfect coverage and limited accuracy become less limiting, provided that the average score is not affected by systematic biases in coverage and accuracy. Thus, methylome coverage and accuracy in methylation calls are a function of resolution.

Only CpGs interrogated in common can be compared directly. The intersections of CpGs covered by the four methods were therefore determined (**Fig. 1c**). Overall, at the sequencing depth investigated, MethylC-seq provided the highest CpG coverage at 95% followed by MeDIP-seq at 67% and MBD-seq at 61%. RRBS covered the fewest CpGs genome-wide (12%), which drove the overlap of all methods to 6% of genome-wide CpGs.

For any given method, how deeply to sequence the library is an open question. As the sequencing depth increases, the number of unique reads covering a particular region approaches the total possible reads present in the library for each enriched region. This saturation occurs when further sequencing fails to discover additional regions above background. To understand the extent to which we sampled the regions represented in the RRBS, MeDIP-seq and MBD-seq libraries, saturation analysis was performed. RRBS approaches but does not reach saturation at the current sequencing depth (**Supplementary Fig. 7a**). For MeDIP-seq and MBD-seq, saturation was observed when false-discovery rate thresholds were applied, but not when unthresholded data were plotted (**Supplementary Fig. 7b,c**). Saturation was not observed for MRE-seq (**Supplementary Fig. 7d,e**), although the average restriction site was represented 13 times within each library, indicating that additional reads would mostly re-sample restriction sites already interrogated. Sequencing beyond saturation improves confidence in the observations and increases the CpG coverage, though at greater cost per CpG covered. Thus, sequencing below or up to saturation maximizes the number of samples that can be analyzed, whereas sequencing beyond saturation maximizes CpG coverage and improves confidence in methylation calls.

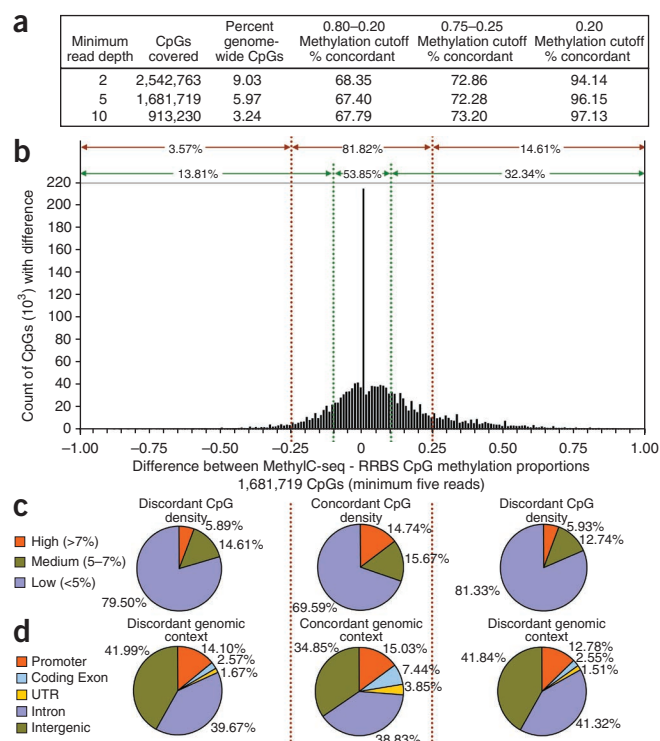
Comparison of bisulfite-based methods

Several observations from the CpG coverage analysis of MethylC-seq and RRBS are important to consider before assessing their concordance in methylation calls. First, RRBS provides substantial coverage of CpGs in CpG islands, but low CpG coverage genome-wide (**Fig. 1a,b**). In contrast, MethylC-seq offers greater CpG coverage genome-wide. When coverage is normalized to 1 Gbp of sequence in the methylome map, RRBS shows higher coverage of CpGs in CpG islands at all read depths (**Supplementary Fig. 5**). This difference points to RRBS as the method of choice if CpG islands are the main focus of a study. However, at lower read thresholds, MethylC-seq sampled far more CpGs in CpG islands than RRBS (**Fig. 1b**).

A major advantage of bisulfite-based methods is that they allow quantitative comparisons of methylation levels at single-base

resolution. For MethylC-seq and RRBS, we calculated and compared the proportion of methylated reads at individual CpGs genome-wide. High concordance was observed using a simple method that makes methylation status calls at different minimum read depths and allows multiple methylation value cutoffs to be examined (**Fig. 2a**). The difference in methylation proportions between MethylC-seq and RRBS at a minimum read depth of 5 was calculated for individual CpGs and concordance was declared if the difference did not exceed a given threshold (**Fig. 2b**). Of the CpGs compared between MethylC-seq and RRBS just 12.75% displayed identical methylation level or a difference threshold of zero. If the difference threshold is relaxed to 0.1 or 0.25, the concordance increased to 53.85% or 81.82%, respectively. This analysis was also performed at minimum read depths of 2 and 10 (**Supplementary Fig. 8a,b**), which, for the 0.25 threshold, showed concordance of 80.28% and 83.89%, respectively, demonstrating that read depth has only a modest effect on concordance. We also performed this analysis for MethylC-seq on replicate no. 3 compared to RRBS on replicate nos. 1 and 2, which showed a similar concordance (79.64% for nos. 3 and 1; 82.95% for nos. 3 and 2) (**Supplementary Fig. 8c-f**). The concordance between MethylC-seq and RRBS both on replicate no. 3, (81.82%), falls between the concordances for different replicates. RRBS on replicate nos. 1 and 2 was also compared (**Supplementary Fig. 8g,h**) and showed a higher concordance (91.54%) than any of the comparisons between MethylC-seq and RRBS, consistent with their high correlation coefficient (**Supplementary Fig. 2**). The RRBS and MethylC-seq discordant calls were not attributable to the local CpG density or genomic context of the individual CpGs (**Fig. 2c,d**). Taken together, these analyses suggest that differences between replicates are attributable to technical or stochastic factors as well as modest biological variation.

Given the notable presence of non-CpG cytosine methylation in H1 ESCs⁸, we also examined concordance between MethylC-seq and RRBS at CHH and CHG cytosines. Because CHH sites are asymmetric with respect to strand and 98% of CHG sites are hemi-methylated⁸, reads mapping to each strand were considered separately. When non-CpG cytosines were considered, either with (**Supplementary Fig. 9**) or without the zero (lack of methylation) methylation percentage (**Supplementary Fig. 10**), concordance was higher than concordance at CpGs. However, a lower degree of variation at non-CpG sites is expected because of the relatively narrow range of methylation levels for non-CpG sites.



For both CpG (Fig. 2b) and non-CpG cytosine (Supplementary Figs. 9 and 10) methylation, MethylC-seq showed slightly higher methylation proportions than RRBS on the same DNA, as demonstrated by the longer tail on the positive side of the graphs. This trend was also observed in comparisons of MethylC-seq to RRBS performed on replicate nos. 1 and 2 (Supplementary Fig. 8c–f), suggesting that technical aspects are driving this difference.

Comparison of methylated-cytosine enrichment methods

Concordance analyses for enrichment methods differ from bisulfite methods in two fundamental ways. First, binary methylation calls are used in enrichment methods, because methylation levels are not easily determined. Second, because of the lack of single CpG resolution inherent in enrichment methods, a windows-based approach is used. The windows can include CpGs that are not directly covered by a read. Thus the percent of genome-wide CpGs contained in the compared windows is naturally higher than the percent of individual CpGs that overlap in the coverage comparison (Fig. 1c). We therefore assessed concordance between MeDIP-seq and MBD-seq by comparing binary highly methylated and weakly methylated calls from the average methylation across 1,000- and 200-bp windows (Online Methods). For both window sizes, concordance was >90% at all read depths examined and improved with increasing minimum read depths (Fig. 3a). We confirmed the concordance between MeDIP-seq and MBD-seq at selected loci by bisulfite treatment of the DNA, PCR, cloning and sequencing (Supplementary Fig. 11 and Supplementary Table 3). The substantially higher concordance relative to the bisulfite-based methods is in part related to the inference common to both enrichment methods that neighboring CpGs within a given window have similar methylation levels and to the binary rather than quantitative methylation calls.

When applied in the context of the enrichment methods, the minimum read depths limit the analysis to regions with at least a minimal methylation level. At sufficiently high sequencing depth, however, greater confidence can be placed in the lack of methylation inferred

Figure 2 Comparison of bisulfite-based methods. (a) Calls of highly/partially/weakly methylated (0.80–0.20 or 0.75–0.25 cutoff) or highly/weakly methylated (0.20 cutoff) were made for CpGs covered at several minimum read depths by MethylC-seq and by RRBS (both on replicate no. 3). The number and percent of genome-wide CpGs covered and the percent of concordant calls are shown for each minimum read depth and methylation call cutoff. (b) Differences (MethylC-seq - RRBS) in methylated proportions (methylated reads/(methylated reads + unmethylated reads)) for CpGs with a minimum coverage of five reads by both methods. Percentages of concordant and discordant methylation were determined at cutoffs of ± 0.1 (green dashed lines) and ± 0.25 (red dashed lines). (c,d) CpG density in a 400-bp window (c) and genomic context of concordant and discordant CpGs at the 0.25 cutoff (d).

from lack of reads. However, at lower sequencing depth, lack of methylation cannot be distinguished from lack of coverage due to the stochastic nature of read coverage. This is an important difference from the bisulfite-based methods, which can identify unmethylated regions at a sequencing depth well below saturation.

The 1,000-bp windows covered at a minimum read depth of 5, representing 99.8% concordance, were examined for potential biases related to CpG density (Fig. 3b) and genomic context (Fig. 3c) on concordance between MeDIP-seq and MBD-seq calls. Concordant and discordant calls were similar in their genomic context, but discordant calls were shifted toward regions of lower CpG density compared to concordant calls. Thus, although these two methods differ in the extent of CpG coverage and read depth at sites covered (Fig. 1a), in windows with even minimal coverage by both methods, the concordance is exceptionally high. To further examine the accuracy of the calls, we compared the methylation calls from MeDIP-seq to those from MethylC-seq. For regions with methylation detectable by MethylC-seq, MeDIP-seq and MBD-seq, calls of highly methylated were made in nearly every case (Fig. 3d).

To examine the reliability of an enrichment-based method specifically for inferring weakly methylated regions at different CpG densities, we compared MeDIP-seq to MethylC-seq (Supplementary Fig. 4). These analyses and limited validation by pyrosequencing suggest that MeDIP-seq allows accurate inferences of lack of methylation and/or weak methylation in regions of high and medium CpG density, whereas accuracy is moderately reduced in regions of low CpG density. Thus, increasing the sequencing depth of MeDIP-seq or using a complementary methodology targeting unmethylated CpGs may be useful.

Although MeDIP-seq and MBD-seq methylation calls are highly concordant in sequences represented in both data sets, interesting differences exist between the regions each interrogates, and the sensitivity of each method to detect non-CpG methylation. First, the rate of enrichment differs slightly with respect to local CpG density, with MeDIP-seq enriching more at regions with relatively low CpG density and MBD-seq enriching more at regions with slightly higher CpG density (Supplementary Fig. 6), which is also reflected in their moderate (46.33%) overlap in CpG coverage. This substantial amount of non-overlap suggests that methylated fragments with low CpG density may bind more efficiently to the 5-methylcytosine antibody, or alternatively, these fragments may be selectively eliminated during enrichment in MBD-seq, depending on the salt concentration used to elute the DNA.

Second, the ability of MeDIP-seq or MBD-seq to detect non-CpG methylation could be particularly important for evaluating the methylome of ESCs, which contains abundant non-CpG methylation⁹. To address this, we examined read densities in gene bodies with similar CpG methylation levels but different CHG methylation

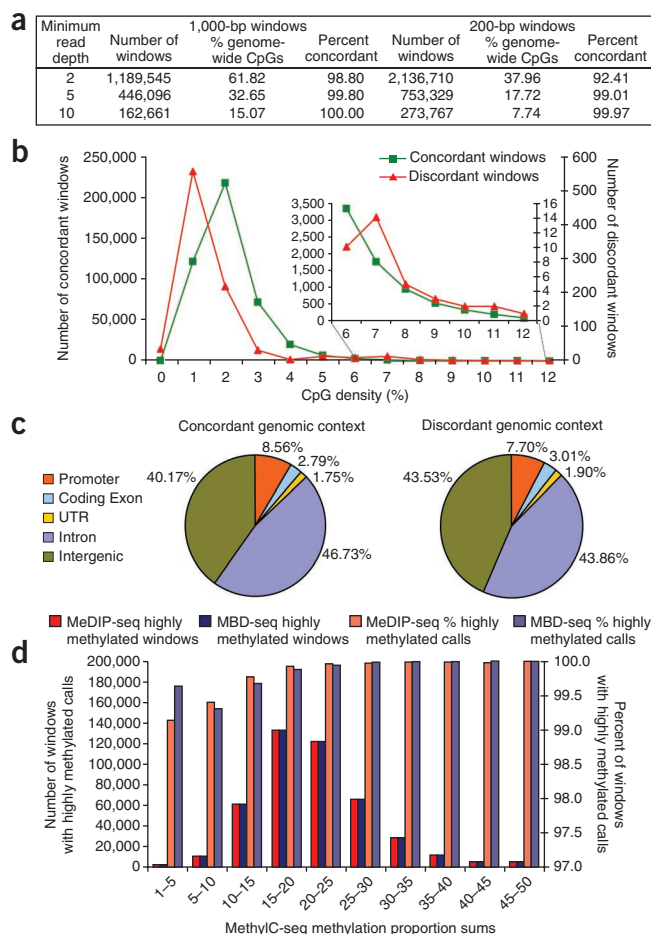


Figure 3 Comparison of methylated DNA enrichment methods. **(a)** Calls of highly/weakly methylated were made by averaging methylation scores for CpGs covered at varying minimum read depths by MeDIP-seq or MBD-seq in 1,000- and 200-bp windows. The number of windows, percent of genome-wide CpGs covered and the percent of concordant calls are shown for each minimum read depth and window size. **(b,c)** For the 1,000-bp windows with a minimum read depth of 5, the CpG density **(b)** and genomic context **(c)** of the concordant and discordant windows are shown. The inset in **b** shows a close-up of the concordance/discordance of CpG densities consistent with CpG islands. **(d)** For the 1,000-bp windows with a minimum read depth of 5, MethylC-seq methylation proportions for CpGs and non-CpG cytosines covered at a minimum read depth of 5, 444,590 windows, were summed and the windows were binned by the sum. For each of these bins, the number of windows called highly methylated by MeDIP-seq or MBD-seq is shown on the left y-axis and the percent of total windows with calls of highly methylated is shown on the right y-axis. Windows with a MethylC-seq methylation proportion sum >15, representing 83% of all windows, were called highly methylated by MeDIP-seq and MBD-seq in 99.9% of cases. The windows with a methylation proportion sum of 1–15, representing 17% of all windows, were called highly methylated by MeDIP-seq and MBD-seq in at least 99.1% of cases.

methods without inferring an unmethylated state from complete absence of reads in enrichment methods, the comparison excluded regions lacking reads.

Methylation calls were made for 1,000-bp windows where all of the methods had at least one CpG covered by a minimum of five or ten reads, allowing for comparison of 199,438 or 87,363 windows, respectively. Of all the windows covered by a minimum of five reads, 2.45% completely encompassed CpG islands and 5.5% overlapped with CpG islands. The four-way comparison revealed a high degree of concordance of methylation calls among all methods (**Fig. 4a,b** and **Supplementary Table 4**). To investigate the effect of applying different highly/weakly methylated cutoffs to MethylC-seq and RRBS, we performed the four-way comparison at several cutoffs (**Supplementary Fig. 14**). Concordance remained >90% up to a highly/weakly methylated cutoff of 0.55, suggesting the concordance results we report are applicable to a wide range of methylation call cutoffs. This result is congruent with the known partitioning of the genome into methylated and unmethylated zones.

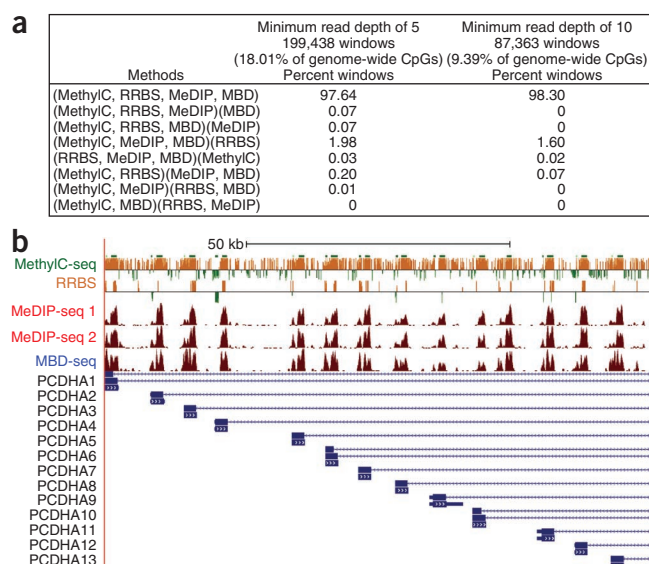
As the limited coverage by RRBS constrained the number of windows that could be compared, a three-way comparison excluding RRBS was also performed. This allowed for the comparison of 444,494 1,000-bp windows or 32% of CpGs genome-wide compared to 18% in the four-way comparison, which showed a three-way concordance of 99.69%. Using different minimum read depth and window sizes had little effect on concordance (**Supplementary Table 5a,b**).

To further evaluate the performance of the four methods, we compared them individually to the widely used Infinium bead-array. For the bisulfite-based methods, the differences in methylation for individual CpGs compared to beta values from the array assaying replicate no. 3 were calculated. At a difference threshold of 0.25, high concordance was observed between the array and MethylC-seq (96.41%; 20,885 CpGs) and between the array and RRBS (97.31%; 5,475 CpGs) (**Supplementary Fig. 15**). For the enrichment-based methods, the average methylation score was calculated for CpGs covered by a minimum of five reads in 200-bp windows centered on CpGs assayed by the array and used to make the binary methylation call. For the array assaying replicate no. 2, highly methylated was defined as >0.20 beta value and weakly methylated defined as ≤0.20 beta value. Both MeDIP-seq (96.19%; 4,960 windows) and MBD-seq (90.80%; 4,163 windows) calls showed high concordance with the array. This high degree of agreement between very different methods further supports the validity of comparing methylation profiles across platforms.

levels as measured by MethylC-seq. MeDIP-seq signal increased with increasing non-CpG cytosine methylation, whereas MBD-seq did not (**Supplementary Fig. 12**), suggesting a differential sensitivity in these two enrichment methods. However, the power to distinguish CpG methylation signal from CHG methylation signal is low, because non-CpG cytosine methylation is often embedded within regions with high CpG methylation. As a negative control, regions in the genome that contain no CpGs were examined. MeDIP-seq and MBD-seq had only background level reads, consistent with the non-CpG cytosines being unmethylated in these regions (**Supplementary Fig. 13**).

Comparison of all methods

To examine concordance of CpG methylation calls from the two bisulfite-based methods and the two methylation enrichment-based methods, a four-way comparison was performed. This can be viewed as combining the two previous pair-wise comparisons, but with three differences. First, to make the bisulfite-based methods comparable to the highly/weakly methylated categorization of MeDIP-seq/MBD-seq scores, a binary calling scheme was applied with highly methylated defined as >0.20 methylation and weakly methylated defined as ≤0.20 methylation. When this calling scheme for individual CpGs was applied to bisulfite-based data alone, the concordance between methods was 94.14% for two reads, 96.15% for five reads and 97.13% for ten reads. Second, to perform the comparison at the same level of resolution, the methylation proportions for individual CpGs in MethylC-seq and RRBS were averaged across windows. Third, to compare the bisulfite-based methods to the enrichment-based



Integrative method

To increase DNA methylome coverage while maintaining modest sequencing requirements, MeDIP-seq was integrated with MRE-seq¹³. The integration is advantageous because the two methods are largely non-overlapping in the regions they interrogate, and because it allows intermediate methylation states to be identified, which is less reliably using MeDIP-seq alone. The methylation scores from MRE-seq were inversely correlated with MeDIP-seq scores (Fig. 5a). The two methods combined assessed the DNA methylation status at 22 million CpGs, 78% of genome-wide CpGs (Fig. 5b). In regions where MRE-seq scores were high and MeDIP-seq scores were low, the MRE-seq reads corroborate the lack of methylation inferred from the absence of MeDIP-seq reads.

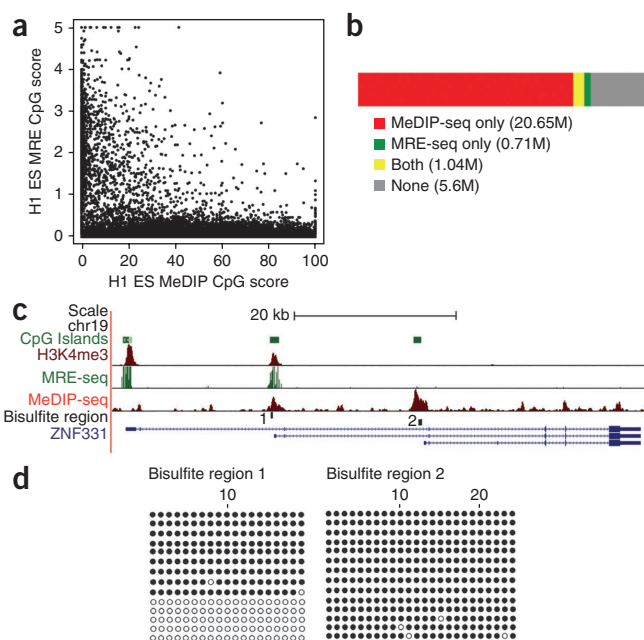
Interestingly, there are a small but significant number of CpG islands with overlapping MeDIP-seq and MRE-seq signals (Supplementary Table 6), indicating an intermediate methylation level. We tested two regions from one locus, *ZNF331*, by clonal bisulfite sequencing (Fig. 5c,d and Supplementary Table 7). Region 1 of *ZNF331* showed overlap of signals from MeDIP-seq and MRE-seq, with bisulfite sequencing confirming intermediate and potentially monoallelic methylation. In contrast, region 2 exhibited MeDIP-seq signal only, and bisulfite sequencing confirmed nearly complete methylation. *ZNF331* exhibits paternal monoallelic expression in multigenerational CEPH pedigrees consistent with imprinting^{25,26}. In addition, allelic

Figure 5 Integrative method increases methylome coverage and enables identification of a DMR. (a) MRE-seq involves parallel digests with methylation-sensitive restriction enzymes (HpaII, AciI and HinfI), selection of cut fragments of ~50–300 bp, pooling the digests, library construction and sequencing. For every 600-bp window along chromosome 21, MeDIP-seq scores were plotted against MRE-seq scores. The plot depicts the inverse relationship between MRE-seq and MeDIP-seq signals. (b) Coverage of CpGs in the human genome by MeDIP-seq alone (red), MRE-seq alone (green), both (yellow) or neither method (no fill). Sequence from replicate nos. 1 and 2 were used in these calculations. (c) UCSC Genome Browser view of *ZNF331* in H1 ESC, showing overlap of MeDIP-seq, MRE-seq and H3K4me3 (from ChIP-seq) signals at bisulfite region 1 and only MeDIP-seq signal at bisulfite region 2. (d) Clonal bisulfite sequencing results for specified regions in ESC from replicate no. 1. A filled circle represents a methylated CpG and an open circle indicates an unmethylated CpG.

Figure 4 Comparison of all methods. (a) The table shows the percentage of 1,000-bp windows with concordant and discordant MethylC-seq (replicate no. 3), RRBS (replicate no. 3), MeDIP-seq (replicate no. 2) and MBD-seq (replicate no. 2) calls at minimum read depths of 5 and 10. Methods making the same call are grouped together in parentheses. Calls were made for MethylC-seq and RRBS by averaging the methylation proportion of CpGs within the window that were covered at the minimum read depth and applying a highly/weakly methylated cutoff of 0.2. Calls were made for MeDIP-seq and MBD-seq by averaging the methylation score of CpGs within the window that were covered at the minimum read depth. (b) Genome browser view of the 100-kb CpG rich Protocadherin alpha cluster (*PCDHA*), exemplifying the significant concordance in methylation status seen on a genome-wide level. For MethylC-seq and RRBS, the y axis displays methylation scores of individual CpGs. Scores range between –500 (unmethylated) and 500 (methylated) and the zero line is equivalent to 50% methylated. Negative scores are displayed as green bars and positive scores are displayed as orange bars. For MeDIP-seq (1), MeDIP-seq (2) and MBD-seq, the y axis indicates extended read density. Browseable genome-wide views of these data sets are available at <http://www.genboree.org/> and <http://genome.ucsc.edu/>.

skewing of DNA methylation at *ZNF331* was reported using SNP arrays²⁷, further supporting a provisional status of *ZNF331* as a novel imprinted gene. Histone H3 lysine 4 trimethylation (H3K4me3), a mark enriched at promoters, overlapped with region 1 but not region 2 (Fig. 5c). A third CpG island at the 5' end of *ZNF331* was fully unmethylated and had an even stronger H3K4me3 peak. Thus, our integrative approach identified a differentially methylated region (DMR) in *ZNF331* that may be a DNA methylation-regulated promoter for one of the *ZNF331* transcripts.

The analysis of *ZNF331* suggested the possibility of using MeDIP-seq and MRE-seq to generate a list of candidate DMRs genome-wide (Supplementary Tables 6 and 7). Ultimately this could define all regions with an intermediate methylation level, encompassing DMRs of all imprinted genes in the genome, or the imprintome, and sites of non-imprinted monoallelic epigenetic regulation. Consistently, our candidate list includes 16 of 19 previously identified DMRs of



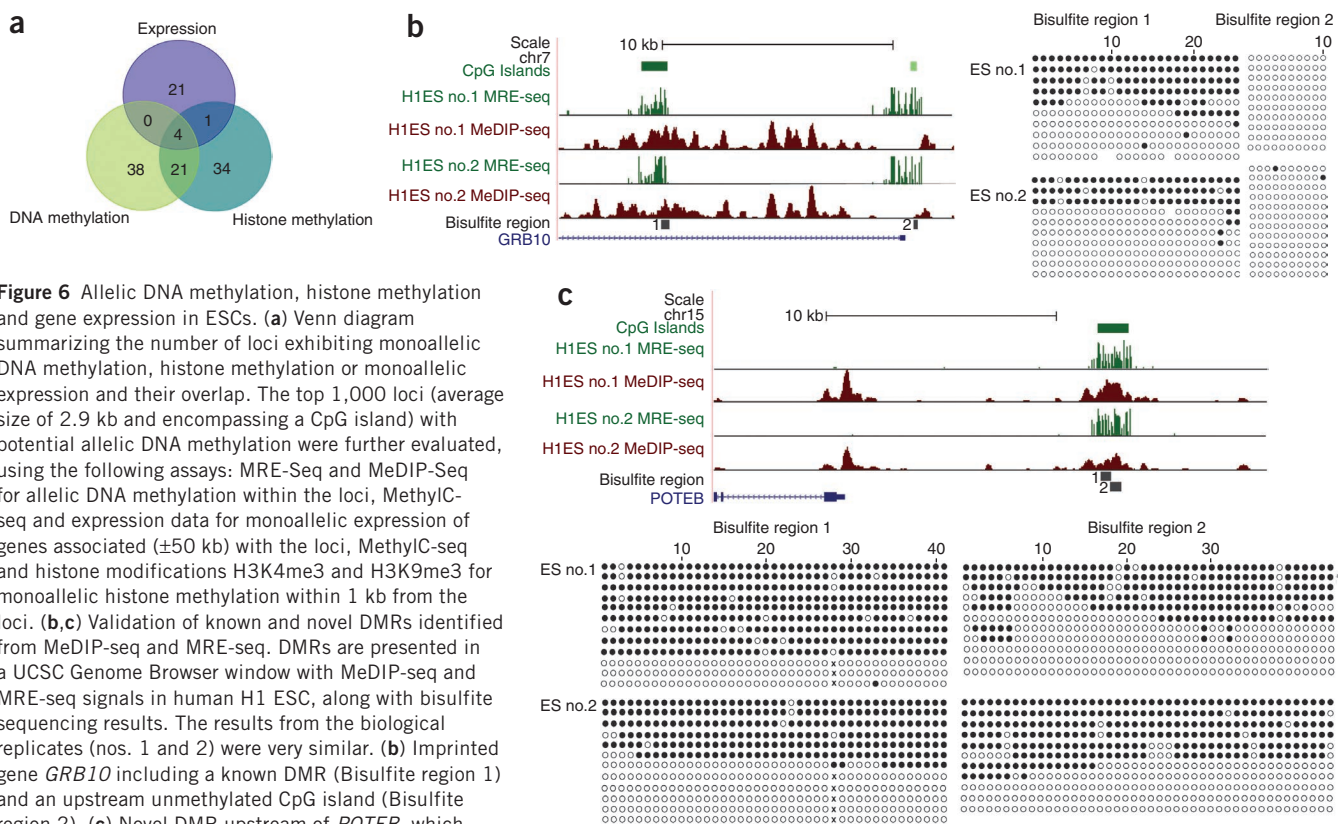


Figure 6 Allelic DNA methylation, histone methylation and gene expression in ESCs. **(a)** Venn diagram summarizing the number of loci exhibiting monoallelic DNA methylation, histone methylation or monoallelic expression and their overlap. The top 1,000 loci (average size of 2.9 kb and encompassing a CpG island) with potential allelic DNA methylation were further evaluated, using the following assays: MRE-Seq and MeDIP-Seq for allelic DNA methylation within the loci, MethylC-seq and expression data for monoallelic expression of genes associated (± 50 kb) with the loci, MethylC-seq and histone modifications H3K4me3 and H3K9me3 for monoallelic histone methylation within 1 kb from the loci. **(b,c)** Validation of known and novel DMRs identified from MeDIP-seq and MRE-seq. DMRs are presented in a UCSC Genome Browser window with MeDIP-seq and MRE-seq signals in human H1 ESC, along with bisulfite sequencing results. The results from the biological replicates (nos. 1 and 2) were very similar. **(b)** Imprinted gene *GRB10* including a known DMR (Bisulfite region 1) and an upstream unmethylated CpG island (Bisulfite region 2). **(c)** Novel DMR upstream of *POTEb*, which exhibits allele-specific DNA methylation. Open circle indicates an unmethylated CpG site. Filled circle represents a methylated CpG site. 'x' indicates absence of a CpG site due to a heterozygous SNP, which destroyed the 28th CpG. All clones without the CpG were unmethylated, whereas all the clones containing the CpG were methylated. Furthermore, the alleles could be distinguished in the sequence reads from MeDIP-seq (G allele, 9 of 9 reads) and MRE-seq (A allele, 30 of 30 reads).

imprinted genes, including *BLCAP*, *GRB10*, *H19*, *INPP5F*, *KCNQ1*, *MEST*, *SGCE*, *SNRPN*, *ZIM2*, *GNAS*, *GNASAS*, *DIRAS3*, *DLK1*, *NDN*, *PLAGL1* and *TP73*. Two of the known DMRs, in *PEG3* and *MEG3*, appeared mostly methylated, potentially representing loss of imprint marks²⁸. One of the 19 known DMRs (for *NAP1L5*) is not within a CpG island but did in fact exhibit intermediate methylation (Supplementary Fig. 16). Thus, extension of this analysis to include CpG-rich regions that are not strictly CpG islands will be useful. The data indicate intermediate DNA methylation states that characterize DMRs within known imprinted regions and others are readily identifiable using an integrative approach.

Monoallelic methylation and gene expression

Sequencing-based methods present a unique opportunity to assign epigenetic marks and gene transcripts to specific alleles. We explored this possibility in the ESCs by identifying SNPs within sequence reads, focusing on the top 1,000 CpG island loci with extensive overlap between MRE-seq and MeDIP-seq signals (Fig. 6a and Supplementary Tables 8 and 9). Of the 1,000 loci examined, 203 contained an informative SNP and 63 of these exhibited monoallelic DNA methylation (Fig. 6a). The remaining 140 of the 203 loci with an informative SNP represent intermediate methylation states that may reflect heterogeneity in methylation across the cell population. In total, 119 of the 1,000 loci exhibited evidence of monoallelic epigenetic modification and/or expression. Four DMRs were identified that were monoallelic in DNA methylation and histone methylation and were associated with a gene exhibiting monoallelic

expression (Supplementary Fig. 17). Strong corroborating evidence for monoallelic DNA methylation was obtained from similar analyses of the MethylC-seq data (Supplementary Fig. 18). These results demonstrate the excellent capabilities of sequencing-based epigenomic and transcriptome assays for identifying genes exhibiting monoallelic epigenetic marks and monoallelic expression.

To further assess the accuracy of methylation status predictions, eight regions (total of 17 nonoverlapping PCR products), which exhibited apparent monoallelic methylation from the MeDIP-seq and MRE-seq SNP analyses (Fig. 6a and Supplementary Table 8) were selected for clonal bisulfite sequencing. Adjacent CpG island loci containing only MRE-seq reads were confirmed to be largely unmethylated (Fig. 6b), whereas loci containing only MeDIP-seq reads were heavily methylated (Supplementary Table 7). Individual bisulfite clones from two known imprinted genes *INPP5F* and *GRB10* were either methylated or unmethylated at nearly all CpGs (Fig. 6b and Supplementary Table 7). *GRB10* exhibited DNA methylation consistent with an isoform-specific imprint mark, as previously reported²⁹. Seven (*BCL8*, *FRG1*, *ZNF331*, *IAH1*, *MEFV*, *POTEb*, *ZFP3*) of the eight putative DMRs showed evidence of differential methylation (Fig. 6c and Supplementary Table 7). Bisulfite analysis of a DMR upstream of *POTEb* at 15q11.2 provided direct evidence for allele-specific methylation (Fig. 6c, lower panel). The H3K9me3 signal at this locus is also monoallelic, as two nucleotides identified as heterozygous from the MethylC-seq reads both showed only a single allele in the H3K9me3 sequence reads (chr15:19346665, T in 4 of 4 reads; and chr15:19348112, C in 13 of 14 reads). In the 150 kb proximal

to *POTEB*, three additional CpG islands exhibit intermediate methylation levels, including one near the noncoding RNA, *CXADRP2* and one encompassing the 5' end of *BCL8*. The allelic pattern of DNA methylation of *BCL8* was confirmed by bisulfite sequencing (Supplementary Table 7).

DISCUSSION

Our quantitative comparison of four sequencing-based DNA methylation methods revealed that all four methods yield largely comparable methylation calls, but differ in CpG coverage, resolution, quantitative accuracy, efficiency and cost. The greater coverage provided by MethylC-seq comes at a >50-fold increase in cost compared to RRBS, MeDIP-seq and MBD-seq. These analyses should be widely useful in understanding the extent to which sequencing-based DNA methylation profiles generated by different methods and different laboratories can be compared to define true biological differences. Given the international investment in mapping human DNA methylomes, and other epigenomic marks, high concordance is essential.

Quantifying differences among the four methods highlighted their strengths and weaknesses. Strengths of bisulfite methods include single-base resolution and an ability to quantify methylation levels. The quantification is imperfect, however, with the methylation level of ~18% of CpG varying by >25% between RRBS and MethylC-seq, and the methylation level of ~5–8% of CpGs varying by >25% in RRBS biological replicates. MethylC-seq is superior in genome-wide CpG coverage, whereas RRBS carries a significantly lower ratio of cost to CpGs covered, particularly at CpG islands. A strength of the enrichment methods is even lower cost per CpG covered genome-wide relative to the bisulfite methods, albeit at reduced resolution. A second potential strength is that in the enrichment methods all four nucleotides are retained, which modestly increases the rate of uniquely mappable sequence reads and permits a greater number of genotype-epigenotype correlations. Enrichment methods do not allow precise quantification of methylation levels, and their methylation calls are therefore fit into two or three categories. Using binary methylation calls, the enrichment methods are remarkably reproducible and highly (99%) concordant, regardless of whether the window size is 200 bp or 1 kb. The inability of enrichment methods to quantify methylation was addressed by integrating MeDIP-seq to map methylated regions with MRE-seq to map unmethylated CpG sites. The integrative approach increases CpG coverage with only a modest increase in cost, and permits accurate identification of intermediate methylation states, such as the methylation states of imprinted genes or cell type-specific methylation within complex tissues. The methods also differ in their abilities to detect methylation at non-CpG cytosines and to discriminate between these residues and CpG methylation. However, the high degree of concordance, approaching 100% between MeDIP-seq and MBD-seq, suggests that this differential ability to detect non-CpG methylation does not have a significant impact on the relative methylation levels within 1,000-bp windows. This observation may be related to the low levels of methylation at non-CpG sites, and their presence in regions with high CpG methylation.

Our finding that MeDIP-seq enriches for regions with lower CpG density compared to MBD-seq is seemingly in contrast to a previous finding³⁰ that MeDIP-seq was more sensitive to regions of high CpG density than MBD-seq. However, it has also been shown³⁰ that increasing eluent salt concentrations in MBD-seq enriches for increasingly higher CpG densities. Our comparison between MeDIP-seq and MBD-seq used a salt concentration of 1 M compared to 700 mM³⁰, which could account for the differences.

Variation in DNA methylation is a topic of wide interest. Variation is observed between individuals, cell and tissue types or within one cell type over time. Our biological replicates displayed variation that was similar in magnitude to variation from limited technical replicates, suggesting the concordance estimates may be marginally higher than what we report. Thus, to identify potentially rare variation in methylation between biological samples, the magnitude of technical variation should be considered.

There are numerous opportunities to increase methylome coverage. First, for RRBS or MRE-seq, for example, selecting additional enzymes, increasing the size range of selected fragments and increasing sequencing depth could dramatically increase CpG coverage. Second, increasing read length or using paired-end sequencing could also positively affect each method. Third, integrative approaches could include MeDIP-seq or MBD-seq coupled with MRE-seq or RRBS, particularly for direct rather than inferred calling of unmethylated CpGs within high CpG density regions. Versatile methods such as 'bisulfite padlock probes' allow more targeted profiling and could also complement the enrichment methods^{14,31}.

Sequencing-based methods are unique in that they allow assessment of the methylation status of repetitive elements, which encompass nearly half of all CpGs in the methylome. The epigenetic status of this entire genomic compartment has been inaccessible to microarrays, but is a critical component of epigenetic gene regulation, as many of the sequences have a regulatory function^{23,32}. Furthermore, the labile DNA methylation status of a particular transposon in the mouse agouti locus influences susceptibility to diabetes and cancer^{33,34}. These and other studies indicate that there is a great deal to be learned about the epigenetic regulation of these abundant but enigmatic elements.

Sequencing-based methylation analysis methods are also unique in that the sequence reads themselves can be used to construct a partial map of genetic variation, including common and rare variants. The comprehensiveness of the genetic map is a function of read coverage and whether reads contain three nucleotides (bisulfite methods) or four nucleotides (enrichment methods). The sites of genetic variation enable local epigenetic states to be associated with specific alleles. SNP microarrays have been similarly deployed for allelic DNA methylation analysis, but the detection of variants is confined to those present on the microarray³⁵. Our combined epigenomic-genomic analyses identified all CpG islands with intermediate methylation states in H1 ESCs, many of which were confirmed as monoallelic DNA methylation, and in some cases, also monoallelic for histone methylation and gene expression. This represents an initial step toward characterizing the human imprintome and genome-wide monoallelic epigenetic states, a goal of basic biological and clinical importance in epigenomic research.

METHODS

Methods and any associated references are available in the online version of the paper at <http://www.nature.com/naturebiotechnology/>.

Data accession. Additional data related to this paper are available at <http://www.genboree.org/java-bin/project.jsp?projectName=Methylation%20Platform%20Comparison&isPublic=yes> and hgdev-remc.cse.ucsc.edu. Data used in this paper are available for download from the GEO NIH Roadmap Epigenomics Project Data Listings (<http://www.ncbi.nlm.nih.gov/geo/roadmap/epigenomics/>) and the Epigenomics Atlas (<http://genboree.org/epigenomeatlas/edaccDataFreeze1.rhtml>).

Note: Supplementary information is available on the Nature Biotechnology website.

ACKNOWLEDGMENTS

We would like to thank the US National Institutes of Health (NIH) Roadmap Epigenomics Program; sponsored by the National Institute on Drug Abuse (NIDA) and the National Institute of Environmental Health Sciences (NIEHS). J.F.C. and M.H. are supported by NIH grant 5U01ES017154-02. A. Milosavljevic is supported by NIH grant 5U01DA025956-02. A. Meissner and B.E.B. are supported by NIH grant 6U01ES017155-02. J.R.E. and B.R. are supported by NIH grant 5U01ES017166-02. R.P.N. was supported by NIH T32 CA108462-04 and F32CA141799. S.L.D. was supported by CIRM TB1-01190. S.D.F. was supported by NIH T32 CA108462-06. B.E.J. was supported by NIH T32 GM008568. M.A.M. is a Terry Fox Young Investigator and a Michael Smith Senior Research Scholar. We thank Z. Zhang and H. Li for modifying the ZOOM algorithm for bisulfite alignments.

AUTHOR CONTRIBUTIONS

J.F.C., R.A.H., T.W., M.H., M.A.M. and A. Milosavljevic conceived and designed the experiments. R.P.N., C.H., S.L.D., B.E.J., S.D.F., Y.Z. and M.H. performed the MeDIP, MRE and bisulfite sequencing experiments. R.A.W. and X.Z. designed and performed pyrosequencing and data analyses. H.G., C.B., A.G. and A. Meissner⁹ performed and analyzed RRBS. L.E., H.O., P.J.F., B.E.B., C.B.E., R.D.H. and B.R. performed and analyzed Chip-seq experiments. R.L., M.P. and J.R.E. analyzed MethylC-seq data and performed Bowtie aligner testing. R.A.H., T.W., K.J.F., J.G., C.C., M.H., X.Z., A.D. and A.O. performed data analysis. T.W., T.B. and D.H. developed MeDIP and methyl-sensitive restriction enzyme scoring algorithms and performed coverage analyses including repetitive sequence analyses. Y.X., W.-Y.C., R.L., M.Q.Z. and W.L. compared bisulfite sequence aligners. J.F.C., R.A.H., M.H., T.W., R.P.N. and R.A.W. wrote the manuscript.

COMPETING FINANCIAL INTERESTS

The authors declare no competing financial interests.

Published online at <http://www.nature.com/naturebiotechnology/>.

Reprints and permissions information is available online at <http://npg.nature.com/reprintsandpermissions/>.

- Robertson, K.D. DNA methylation and human disease. *Nat. Rev. Genet.* **6**, 597–610 (2005).
- Bird, A. DNA methylation patterns and epigenetic memory. *Genes Dev.* **16**, 6–21 (2002).
- Feinberg, A.P. & Vogelstein, B. Hypomethylation distinguishes genes of some human cancers from their normal counterparts. *Nature* **301**, 89–92 (1983).
- Gama-Sosa, M.A. *et al.* Tissue-specific differences in DNA methylation in various mammals. *Biochim. Biophys. Acta* **740**, 212–219 (1983).
- Tahiliani, M. *et al.* Conversion of 5-methylcytosine to 5-hydroxymethylcytosine in mammalian DNA by MLL partner TET1. *Science* **324**, 930–935 (2009).
- Kriaucionis, S. & Heintz, N. The nuclear DNA base 5-hydroxymethylcytosine is present in Purkinje neurons and the brain. *Science* **324**, 929–930 (2009).
- Ito, S. *et al.* Role of Tet proteins in 5mC to 5hmC conversion, ES-cell self-renewal and inner cell mass specification. *Nature* **466**, 1129–1133 (2010).
- Lister, R. *et al.* Human DNA methylomes at base resolution show widespread epigenomic differences. *Nature* **462**, 315–322 (2009).
- Meissner, A. *et al.* Genome-scale DNA methylation maps of pluripotent and differentiated cells. *Nature* **454**, 766–770 (2008).

- Jacinto, F.V., Ballestar, E. & Esteller, M. Methyl-DNA immunoprecipitation (MeDIP): hunting down the DNA methylome. *Biotechniques* **44**, 35–43 (2008).
- Down, T.A. *et al.* A Bayesian deconvolution strategy for immunoprecipitation-based DNA methylome analysis. *Nat. Biotechnol.* **26**, 779–785 (2008).
- Serre, D., Lee, B.H. & Ting, A.H. MBD-isolated Genome Sequencing provides a high-throughput and comprehensive survey of DNA methylation in the human genome. *Nucleic Acids Res.* **38**, 391–399 (2010).
- Maunakea, A.K. *et al.* Conserved role of intragenic DNA methylation in regulating alternative promoters. *Nature* **466**, 253–257 (2010).
- Ball, M.P. *et al.* Targeted and genome-scale strategies reveal gene-body methylation signatures in human cells. *Nat. Biotechnol.* **27**, 361–368 (2009).
- Cokus, S.J. *et al.* Shotgun bisulfite sequencing of the *Arabidopsis* genome reveals DNA methylation patterning. *Nature* **452**, 215–219 (2008).
- Lister, R. *et al.* Highly integrated single-base resolution maps of the epigenome in *Arabidopsis*. *Cell* **133**, 523–536 (2008).
- The American Association for Cancer Research Human Epigenome Task Force European Union, Network of Excellence, Scientific Advisory Board Moving AHEAD with an international human epigenome project. *Nature* **454**, 711–715 (2008).
- Langmead, B., Trapnell, C., Pop, M. & Salzberg, S.L. Ultrafast and memory-efficient alignment of short DNA sequences to the human genome. *Genome Biol.* **10**, R25 (2009).
- Xi, Y. & Li, W. BSMAP: whole genome bisulfite sequence MAPping program. *BMC Bioinformatics* **10**, 232 (2009).
- Coarfa, C. & Milosavljevic, A. Pash 2.0: scaleable sequence anchoring for next-generation sequencing technologies. *Pac. Symp. Biocomput.* **2008**, 102–113 (2008).
- Smith, A.D. *et al.* Updates to the RMAP short-read mapping software. *Bioinformatics* **25**, 2841–2842 (2009).
- Lin, H., Zhang, Z., Zhang, M.Q., Ma, B. & Li, M. ZOOM! Zillions of oligos mapped. *Bioinformatics* **24**, 2431–2437 (2008).
- Wang, T. *et al.* Species-specific endogenous retroviruses shape the transcriptional network of the human tumor suppressor protein p53. *Proc. Natl. Acad. Sci. USA* **104**, 18613–18618 (2007).
- Kunarto, G. *et al.* Transposable elements have rewired the core regulatory network of human embryonic stem cells. *Nat. Genet.* **42**, 631–634 (2010).
- Pant, P.V.K. *et al.* Analysis of allelic differential expression in human white blood cells. *Genome Res.* **16**, 331–339 (2006).
- Pollard, K.S. *et al.* A genome-wide approach to identifying novel-imprinted genes. *Hum. Genet.* **122**, 625–634 (2008).
- Schalkwyk, L.C. *et al.* Allelic skewing of DNA methylation is widespread across the genome. *Am. J. Hum. Genet.* **86**, 196–212 (2010).
- Pick, M. *et al.* Clone- and gene-specific aberrations of parental imprinting in human induced pluripotent stem cells. *Stem Cells* **27**, 2686–2690 (2009).
- Arnaud, P. *et al.* Conserved methylation imprints in the human and mouse *GRB10* genes with divergent allelic expression suggests differential reading of the same mark. *Hum. Mol. Genet.* **12**, 1005–1019 (2003).
- Li, N. *et al.* Whole genome DNA methylation analysis based on high throughput sequencing technology. *Methods* published online, doi: 10.1016/j.ymeth.2010.04.009 (27 April 2010).
- Deng, J. *et al.* Targeted bisulfite sequencing reveals changes in DNA methylation associated with nuclear reprogramming. *Nat. Biotechnol.* **27**, 353–360 (2009).
- Bourque, G. Transposable elements in gene regulation and in the evolution of vertebrate genomes. *Curr. Opin. Genet. Dev.* **19**, 607–612 (2009).
- Duhl, D.M., Vrieling, H., Miller, K.A., Wolff, G.L. & Barsh, G.S. Neomorphic agouti mutations in obese yellow mice. *Nat. Genet.* **8**, 59–65 (1994).
- Waterland, R.A. & Jirtle, R.L. Transposable elements: targets for early nutritional effects on epigenetic gene regulation. *Mol. Cell. Biol.* **23**, 5293–5300 (2003).
- Hellman, A. & Chess, A. Gene body-specific methylation on the active X chromosome. *Science* **315**, 1141–1143 (2007).

¹Department of Molecular and Human Genetics, Baylor College of Medicine, Houston, Texas, USA. ²Center for Genome Sciences and Systems Biology, Department of Genetics, Washington University School of Medicine, St. Louis, Missouri, USA. ³Brain Tumor Research Center, Department of Neurosurgery, Helen Diller Family Comprehensive Cancer Center, University of California San Francisco, San Francisco, California, USA. ⁴Genome Sciences Centre, BC Cancer Agency, Vancouver, British Columbia, Canada. ⁵Center for Biomolecular Science and Engineering, University of California, Santa Cruz, California, USA. ⁶Department of Pharmacology and the Genome Center, University of California-Davis, Davis, California, USA. ⁷Genomic Analysis Laboratory, The Salk Institute for Biological Studies, La Jolla, California, USA. ⁸Division of Biostatistics, Dan L. Duncan Cancer Center, Department of Molecular and Cellular Biology, Baylor College of Medicine, Houston, Texas, USA. ⁹Broad Institute of Harvard and MIT, Cambridge, Massachusetts, USA. ¹⁰Department of Pathology, Massachusetts General Hospital and Harvard Medical School, Boston, Massachusetts, USA. ¹¹Center for Cancer Research, Massachusetts General Hospital, Boston, Massachusetts, USA. ¹²Ludwig Institute for Cancer Research. ¹³Department of Cellular and Molecular Medicine, University of California San Diego, La Jolla, California, USA. ¹⁴Cold Spring Harbor Laboratory, Cold Spring Harbor, New York, USA. ¹⁵Department of Molecular and Cell Biology, Center for Systems Biology, University of Texas at Dallas, Dallas, Texas, USA. ¹⁶Department of Stem Cell and Regenerative Biology, Harvard University, Cambridge, Massachusetts, USA. ¹⁷Harvard Stem Cell Institute, Cambridge, Massachusetts, USA. ¹⁸Max Planck Institute for Informatics, Saarbrücken, Germany. ¹⁹USDA/ARS Children's Nutrition Research Center, Department of Pediatrics, Baylor College of Medicine, Houston, Texas, USA. Correspondence should be addressed to J.F.C. (jcstello@cc.uccsf.edu).

ONLINE METHODS

ESCs. H1 cells were grown in mTeSR1 medium³⁶ on Matrigel (BD Biosciences) for 10 passages on 10 cm² plates and harvested at passage 27. Cells were harvested by scraping before snap freezing for DNA isolation. Cells were also harvested from passages 30 and 32 and divided for isolation of DNA, RNA and chromatin.

Illumina Infinium methylation assay. We used 500 ng genomic DNA per sample for the Infinium methylation assay (Illumina), which measures methylation at 27,578 CpGs, with ~2 probes per gene (14,475 RefSeq genes). Bisulfite conversion was performed with the EZ DNA methylation kit (Zymo Research) and each sample was eluted in 12 µl water. Amplification and hybridization to the Illumina HumanMethylation27 BeadChip were carried out according to manufacturer's instructions at the UCSF Genomics Core Facility. Beta values, representing quantitative measurements of DNA methylation at individual CpGs, were generated with Illumina GenomeStudio software. Beta values were normalized to background and filtered to remove those with low signal intensity. The filtered data were used for all subsequent analysis.

Shotgun bisulfite sequencing (MethylC-seq). As described⁸.

RRBS. RRBS analysis was performed as described previously^{37,38}, using ~30 ng of H1-derived DNA as input. The steps of the experimental protocol were as follows. (i) DNA digestion using the MspI restriction enzyme, which cuts DNA at its recognition site (CCGG) independent of the CpG methylation status. (ii) End repair and ligation of adapters for Illumina sequencing. (iii) Gel-based selection of DNA fragment sizes ranging from 40 bp to 220 bp. (iv) Two successive rounds of bisulfite treatment, after which we observed 98.4% converted cytosines outside of CpGs. Due to the presence of non-CpG methylation in ESCs, this value is an underestimate of the actual bisulfite conversion rate. (v) PCR amplification of the bisulfite-converted library and sequencing on the Illumina Genome Analyzer II according to the manufacturer's protocol.

A total of two lanes were sequenced, and the data were processed using Illumina's standard pipeline for image analysis and base calling. The alignment was performed using custom software developed at the Broad Institute⁹. The non-RepeatMasked reference sequence is generated by size-selecting from an *in silico* digest with the MspI restriction enzyme, and before the alignment all Cs in the reference sequence and in the aligned reads are converted into Ts. The alignment itself uses a straightforward seed-and-extension algorithm, identifying all perfect 12 bp alignments and extending without gaps from either end of the seed. The best alignment is kept only in cases where the second-best alignment has at least three more mismatches, whereas all reads that match multiple times are discarded. The DNA methylation level of a specific CpG is calculated as the number of C-to-C matches between the unconverted reference sequence and the aligned read sequence divided by the sum of number of C-to-C matches and C-to-T mismatches.

MBD-seq. As described above, 3 µg of gDNA isolated was sheared to ~300 bp using the Covaris E210 sonicator (Covaris) and size separated by PAGE (8%). The 200- to 400-bp DNA fraction was excised, eluted overnight at 4 °C in 200 µl of elution buffer (5:1, LoTE buffer (3 mM Tris-HCl, pH 7.5, 0.2 mM EDTA)-7.5 M ammonium acetate) and purified using a QIAquick purification kit (Qiagen). The size selected DNA was end-repaired, A-tailed and ligated to 2.5 mMol of 'paired-end' adapters (IDT) following the manufacturer's recommended protocol (Illumina). The resulting product was purified on a QIAquick MinElute column (Qiagen) and assessed and quantified using an Agilent DNA 1000 series II assay and Qubit fluorometer (Invitrogen), respectively. 100 ng of pre-adapted, size-selected product was subjected to immunoprecipitation using the MethylMiner Methylated DNA Enrichment Kit (Invitrogen) following the manufacturer's recommended protocol. The bound fraction was eluted at 600 mM, 1 M and 2 M NaCl and concentrated by the addition of 1 µl (20 µg/µl) mussel glycogen, 1/10th v/v 3 M sodium acetate (pH 5.2) and 2x v/v 100% ethanol. Samples were incubated at -80 °C for 2 h and subsequently centrifuged for 15 min at 16,000g at 4 °C. Pellets were washed with 500 µl cold 70% ethanol two times with 5 min centrifugation at 16,000g at 4 °C between washes and resuspended in 60 µl nuclease-free water. After purification eluted products were subjected to PCR using Illumina paired-end

adapters (Illumina.) with 15 cycles of PCR amplification. PCR products were purified on QIAquick MinElute columns (Qiagen) and assessed and quantified using an Agilent DNA 1000 series II assay and size separated by PAGE (8%). The 320- to 520-bp DNA fraction was excised and purified as described above. The products were assessed and quantified using an Agilent DNA 1000 series II assay and Qubit fluorometer (Invitrogen), respectively. A 1 µl aliquot of each library was used as template in two independent PCR reactions to confirm enrichment for methylated (*SNRPN* promoter) and de-enrichment for unmethylated (CpG-less sequence on Chr15)¹³ for primer sequences). Cycling was 95 °C for 30 s, 55 °C for 30 s and 72 °C for 30 s with 30 cycles. PCR products were visualized by 1.8% agarose gel electrophoresis. Each library was diluted to 8 nM for sequencing on an Illumina Genome Analyzer following the manufacturer's recommended protocol.

MeDIP-seq. As described above 2–5 µg DNA isolated was sonicated to ~100–500 bp with a Bioruptor sonicator (Diagenode). Sonicated DNA was end-repaired, A-tailed and ligated to adapters following the standard Illumina protocol. After agarose size-selection to remove unligated adapters, adaptor-ligated DNA was used for each immunoprecipitation using a mouse monoclonal anti-methylcytidine antibody (1 mg/ml, Eurogentec). DNA was heat denatured at 95 °C for 10 min, rapidly cooled on ice and immunoprecipitated with 1 µl primary antibody per microgram of DNA overnight at 4 °C with rocking agitation in 500 µl immunoprecipitation (IP) buffer (10 mM sodium phosphate buffer, pH 7.0, 140 mM NaCl, 0.05% Triton X-100). To recover the immunoabsorbed DNA fragments, 1 µl of rabbit anti-mouse IgG secondary antibody (2.5 mg/ml, Jackson ImmunoResearch) and 100 µl Protein A/G beads (Pierce Biotechnology) were added and incubated for an additional 2 h at 4 °C with agitation. After immunoprecipitation a total of 6 IP washes were performed with ice cold IP buffer. A nonspecific mouse IgG IP (Jackson ImmunoResearch) was performed in parallel to methyl DNA IP as a negative control. Washed beads were resuspended in TE with 0.25% SDS and 0.25 mg/ml proteinase K for 2 h at 55 °C and then allowed to cool to 25 °C. MeDIP and supernatant DNA were purified using Qiagen MinElute columns and eluted in 16 µl elution buffer (EB) (Qiagen). Fifteen cycles of PCR were performed on 5 µl of the immunoprecipitated DNA using the single-end Illumina PCR primers. The resulting reactions are purified over Qiagen MinElute columns, after which a final size selection (220–420 bp) was performed by electrophoresis in 2% agarose. Libraries were quality checked by spectrophotometry and Agilent DNA Bioanalyzer analysis, which indicated an average fragment size of 150 bp. An aliquot of each library was diluted in EB to 5 ng/µl and 1 µl used as template in four independent PCR reactions to confirm enrichment for methylated and de-enrichment for unmethylated sequences, compared to 5 ng of input (sonicated DNA). Two positive controls (*SNRPN* and *MAGEA1* promoters) and two negative controls (a CpG-less sequence on Chr15 and *GAPDH* promoter) were amplified¹³ for primer sequences). Cycling was 95 °C for 30 s, 58 °C for 30 s, 72 °C for 30 s with 30 cycles. PCR products were visualized by 1.8% agarose gel electrophoresis.

Calculating MeDIP-seq and MBD-seq scores for single CpGs. MeDIP-seq and MBD-seq reads were mapped to the non-RepeatMasked human genome assembly (hg18) with Mapping and Assembly with Quality (MAQ). An algorithm was developed to calculate methylation scores for individual CpGs based on MeDIP-seq or MBD-seq data. Each uniquely mapped, non-redundant sequence read was extended to 150 bp long, representing individual DNA fragments pulled down in the methylation enrichment experiment. The algorithm makes two assumptions: first, for a given fragment, this fragment is assigned to a CpG site that is covered by this fragment and the probability of assigning it to a particular CpG, when there is more than 1 CpG is proportional to the level of methylation of the CpG site; the weighted sum of the probability of all CpGs covered by this fragment is always 1. Second, for a given CpG site, the number of fragments assigned to it is proportional to the level of methylation of this CpG site. The algorithm initiates by assigning a score of 1 to all CpGs, and then it iterates through two steps. In the first step, fragments are assigned to CpGs based on their scores. In the first round, because all CpGs have the same score of 1, an equal fraction of a fragment is assigned to each CpG that the fragment covers, and this is done for all fragments. In the second step, all the fractions of reads each CpG received in step 1 are added up, and this weighted sum is

used as a methylation score for this CpG site. Then, the first step is repeated; only now individual CpGs may have a different prior for assigning reads. A fraction of a fragment is now assigned to CpGs that fragment covers based on methylation scores of the CpGs, that is, the fraction assigned to each CpG is proportional to its methylation score. These updated fragment counts are summed again in step 2 and used as methylation score for individual CpGs. The algorithm iterates through these two steps until the methylation scores converge. These scores are in essence CpG density normalized read density.

Methylation sensitive restriction enzyme sequencing (MRE-seq). Three parallel digests were performed (HpaII, AciI and HinfI; Fermentas), each with 1 µg of DNA. Five units of enzyme per microgram DNA were added and incubated at 37 °C in Fermentas “Tango” buffer for 3 h. A second dose of enzyme was added (5 units of enzyme per microgram DNA) and the DNA was incubated for an additional 3 h. Digested DNA was precipitated with sodium acetate and ethanol and 500 ng of each digest were combined into one tube. Combined DNA was size-selected by electrophoresis on a 1% agarose TBE gel. A 100–300 bp gel slice was excised using a sterile scalpel and gel-purified using Qiagen Qiaquick columns, eluting in 30 µl of Qiagen EB buffer. Library construction was performed using the Illumina Genomic DNA Sample Kit (Illumina) with single-end adapters, following the manufacturer’s instructions with the following changes. For the end-repair reaction, T4 DNA polymerase and T4 polynucleotide kinase were excluded and the Klenow DNA polymerase was diluted 1:5 in water and 1 µl used per reaction. For single end oligo adaptor ligation, adaptors were diluted 1:10 in water and 1 µl used per reaction. After the second size selection, DNA was eluted in 36 µl EB buffer using Qiagen Qiaquick columns, and 13 µl used as template for PCR, using Illumina reagents and cycling conditions with 18 cycles. After cleanup with Qiagen MinElute columns, each library is examined by spectrophotometry (Nanodrop, Thermo Scientific) and Agilent DNA Bioanalyzer (Agilent).

Methyl-sensitive restriction enzyme scores. MRE-seq reads were mapped to the human genome assembly (hg18) with MAQ with an additional constraint that the 5’ end of a read must map to the CpG site within a methyl-sensitive restriction enzyme site. An MRE-score was defined for each CpG site as the number of MRE-reads that map to the site, regardless of the orientation, normalized by the number of million reads generated by the specific enzyme. An MRE-score for each genomic window (e.g., any given 600 bp window) was defined as the average MRE-score for all CpGs that have a score within the window.

RNA-seq. Polyadenylated RNA was purified from 20 µg of DNaseI (Invitrogen)-treated total RNA using the MACS mRNA Isolation Kit (Miltenyi Biotec). Double-stranded cDNA was synthesized from the purified polyA⁺ RNA using Superscript Double-Stranded cDNA Synthesis kit (Invitrogen) and random hexamer primers (Invitrogen) at a concentration of 5 µM. The resulting cDNA was sheared using a Sonic Dismembrator 550 (Fisher Scientific) and size separated by PAGE (8%). The 190–210 bp DNA fraction was excised, eluted overnight at 4 °C in 300 µl of elution buffer (5:1, LoTE buffer (3 mM Tris-HCl, pH 7.5, 0.2 mM EDTA)-7.5 M ammonium acetate) and purified using a QIAquick purification kit (Qiagen). The sequencing library was prepared following the Illumina Genome Analyzer paired end library protocol (Illumina) with 10 cycles of PCR amplification. PCR products were purified on Qiaquick MinElute columns (Qiagen) and assessed and quantified using an Agilent DNA 1000 series II assay and Qubit fluorometer (Invitrogen) respectively. The resulting libraries were sequenced on an Illumina Genome Analyzer_{ix} following the manufacturer’s instructions. Image analysis and base calling was performed by the GA pipeline v1.1 (Illumina) using phasing and matrix values calculated from a control phiX174 library run on each flowcell.

ChIP-seq. Protocols for the chromatin immunoprecipitation assay and Illumina library construction are described in details elsewhere³⁹. Briefly, cross-linked hESCs were obtained from Cellular Dynamics, chromatin was extracted and sonicated to an average size of 500 bp. Individual ChIP assays were performed using 50 µg chromatin (equivalent to 5 × 10⁶ cells) and 2 µg of antibody were added to each ChIP reaction. The histone antibodies used in this study include H3AcK9 (Millipore), H3me3K4 (CST), H3me3K27

(CST), H3me3K9 (Abcam), H3me3K36 (Abcam) and H3me1K4 (Abcam5). ChIP libraries have been created⁴⁰ using the entire purified ChIP sample. All ChIP samples except H3me1K4 were amplified using paired-end Illumina primers for a total of 18 cycles. Libraries were then run on a 2% agarose gel, and the 150- to 500-bp fraction of the library was extracted and purified. The H3me1K4 library was constructed by performing size selection of the 200- to 400-bp library fragment before a 15-cycle amplification. The libraries were quantified using a BioAnalyzer and sequenced. ChIP-seq peaks were called using the Sole-Search software⁴¹.

Bisulfite pyrosequencing. Site-specific analysis of CpG methylation was performed by bisulfite pyrosequencing. Genomic DNA (1.0 µg) was bisulfite modified and pyrosequencing was performed as previously described⁴². The quantitative performance of each pyrosequencing assay was verified by measuring methylation standards comprised of known proportions of unmethylated (whole genome-amplified) and fully methylated (SssI-treated) genomic DNA⁴³.

Comparison was performed on three combinations of DNA methylome platforms: MethylC-seq versus reduced representation bisulfite sequencing (RRBS) and MethylC-seq versus methylated DNA immunoprecipitation sequencing (MeDIP-seq). H1 cell lines of different passage number were used in these experiments (Batch 3 for MethylC-seq, Batch 1 for RRBS and MeDIP). CpGs showing > 80% difference in methylation for the MethylC-seq – RRBS comparison or > 80% difference between the methylated proportion and the methylation score for MethylC-seq and MeDIP comparisons were identified and regions with clusters of these sites were identified for pyrosequencing. Based on the distribution of target CpGs we looked for genomic regions with appropriate length (within range 50 bp to 75 bp), few or no non-CG cytosines and 2 or many target CpGs. Pyrosequencing assays were designed and carried out in 16 regions selected for validation; 14 of these yielded reliable results. Genomic coordinates and primers used for pyrosequencing for the validated regions are listed in **Supplementary Table 1**.

Clonal bisulfite sequencing. Further validation of genome-wide data, particularly sites with apparent allelic DNA methylation, was performed by bisulfite sequencing. Total genomic DNA underwent bisulfite conversion following established protocol⁴⁴ with a modified conversion conditions of: 95 °C for 1 min, 50 °C for 59 min for a total of 16 cycles. Bisulfite PCR primers (**Supplementary Table 4**) were used to amplify regions of interest and were subsequently cloned using pCR2.1/TOPO (Invitrogen). Single colony PCR and sequencing (QuintaraBio) provided contigs that were aligned for analysis.

Data analyses. Comparison of CpG or non-CpG site methylation. Repeat masking of the reference genome assembly was not used in any of these analyses. For bisulfite-based methods, reads that mapped to the positive and negative strand were combined for CpG methylation calculations, but not for CHG and CHH methylation calculations due to the strand asymmetry of non-CpG methylation⁹. The methylated proportion was calculated for each CpG or non-CpG as (methylated reads/(methylated reads + unmethylated reads)). Comparisons of methylation status calls were performed by imposing minimum requirements of 2, 5 or 10 reads covering a CpG or non-CpG site and applying varying methylated proportion cutoffs (0.80–0.20, 0.75–0.25 or 0.20) to make calls on the methylation status. Methylated proportion differences were calculated as (MethylC-seq proportion - RRBS proportion). Methylation proportion difference graphs were generated by counting the number of CpGs with a particular methylated proportion difference and plotting the count on the y-axis. Concordance was then calculated as the percent of CpGs with a methylation proportion difference less than 0.1 or 0.25.

For enrichment-based methods, methylation scores inferred for individual CpGs were averaged across CpGs covered by a varying minimum number of reads in 1,000- or 200-bp windows. Methylation calls of highly methylated (methylation score >8) or weakly methylated (methylation score ≤8) were made based on the average methylation score for each window where at least one CpG was covered by the minimum number of reads.

Genomic context of concordant and discordant CpGs. The overlap of concordant and discordant CpGs with annotated genes, as defined by the UCSC Genome Browser RefSeq Gene track (2010-01-24 version

<http://genome.ucsc.edu/cgi-bin/hgTrackUi?g=refGene>), was identified. To deal with overlapping genes and multiple isoforms of genes, CpGs were classified into gene components based on the following prioritization order: Promoter (within 8,000 bp upstream of a transcription start site), Coding Exon, UTR and Intron. CpGs that did not overlap with any of these gene components were identified as Intergenic.

36. Ludwig, T.E. *et al.* Feeder-independent culture of human embryonic stem cells. *Nat. Methods* **3**, 637–646 (2006).
37. Gu, H. *et al.* Genome-scale DNA methylation mapping of clinical samples at single-nucleotide resolution. *Nat. Methods* **7**, 133–136 (2010).
38. Smith, Z.D., Gu, H., Bock, C., Gnirke, A. & Meissner, A. High-throughput bisulfite sequencing in mammalian genomes. *Methods* **48**, 226–232 (2009).
39. O'Geen, H., Fietze, S. & Farnham, P.J. Using ChIP-seq technology to identify targets of zinc finger transcription factors. *Methods Mol. Biol.* **649**, 437–455 (2010).
40. Robertson, G. *et al.* Genome-wide profiles of STAT1 DNA association using chromatin immunoprecipitation and massively parallel sequencing. *Nat. Methods* **4**, 651–657 (2007).
41. Blahnik, K.R. *et al.* Sole-Search: an integrated analysis program for peak detection and functional annotation using ChIP-seq data. *Nucleic Acids Res.* **38**, e13 (2010).
42. Waterland, R.A., Lin, J., Smith, C.A. & Jirtle, R.L. Post-weaning diet affects genomic imprinting at the insulin-like growth factor 2 (Igf2) locus. *Hum. Mol. Genet.* **15**, 705–716 (2006).
43. Shen, L., Guo, Y., Chen, X., Ahmed, S. & Issa, J.J. Optimizing annealing temperature overcomes bias in bisulfite PCR methylation analysis. *Biotechniques* **42**, 48, 50, 52 passim (2007).
44. Grunau, C., Clark, S.J. & Rosenthal, A. Bisulfite genomic sequencing: systematic investigation of critical experimental parameters. *Nucleic Acids Res* **29**, E65 (2001).